COMPREHENSIVE ASSESSMENT OF BILGE KEELS AND FINS FOR ENHANCING WIND-POWERED VESSEL PERFORMANCE: BRIDGING LABORATORY INSIGHTS TO OPERATIONAL EFFICIENCY

G. Jacobi, Delft University of Technology, Netherlands
N.J. van der Kolk, AlbatrosDigital, Netherlands

SUMMARY

This study delves into the effectiveness of bilge and fin keels, exploring their impacts on the efficiency of wind-powered vessels. Employing Particle Image Velocimetry (PIV) in a towing tank configuration, the research systematically analyses flow features generated by these keels and quantifies the hydrodynamic forces across various bilge and fin keel geometries. Building on prior research, this investigation extends its scope by tracking the path of shed vortices towards the propeller plane and evaluating the tested appendage configurations along global shipping routes. A comprehensive digital ship modelling is composed using the Albatros Software, incorporating laboratory measurements for hydrodynamic coefficients and vorticity induced effects. The impact of these keel types on ship performance in terms of aerodynamics and net propuslive contributions is presented and discussed. Results from laboratory experiments reveal distinct mechanisms through which each appendage type enhances hydrodynamic performance while at the same time identifying certain damaging interaction effects, providing valuable insights for future design optimizations.

NOMENCLATURE

A nomenclature is required for papers/technical notes using a large number of symbols, abbreviations and acronyms. SI units should be used wherever possible and ordered alphabetically.

ρ_air	Air density (kg m^{-3})
ρ_$water$	Seawater density (kg m^{-3})
β	Leeway angle (deg)
ϕ	Heel angle (deg)
C_X	Non-dimensional hydrodynamic surge force $C_X = X/(1/2\ \rho V\text{^}2\ LT)$ (-)
C_Y	Non-dimensional hydrodynamic sway force $C_Y = Y/(1/2\ \rho V\text{^}2\ LT)$ (-)
C_N	Non-dimensional hydrodynamic yawing moment $C_N = N/(1/2\ \rho V\text{^}2\ L\text{^}2\ T)$ (-)
CLR	Centre of lateral resistance $CLR = N/Y$ (-)
COE	Aerodynamic centre of effort (-)
F_WPS	Aerodynamic thrust (kgms^{-2})
N_β	Linear manoeuvring coefficient for yaw (-)
N_βββ	Non-linear manoeuvring coefficient for yaw (-)
L	Length Waterline of the ship (m)
LOA	Length Over All of the ship (m)
P_WPS	Equivalent propulsive power provided by wind propulsion system (kW)
P_WPS *	Non-dimensional WPS P_{WPS} *= P_{WPS}/(1/2 ρ_air $(LOA{\cdot}Span)TWS\text{^}3$) (-)
Span	Height of wind propulsion system (m)
T	Ship draft (m)
TWA	True Wind Angle (deg)
TWS	True Wind Speed (deg)
V	Ship speed (ms^{-1})
WPS	Wind Propulsion System
X_ββ	Quadratic manoeuvring coefficient for surge (-)
Y_β	Linear manoeuvring coefficient for sway (-)
Y_βββ	Non-linear manoeuvring coefficient for sway (-)

1. INTRODUCTION

To counteract aerodynamic forces, additional appendages can help maintain stability and reduce rudder angle. Small appendages, such as those similar to stabilizer fins, are often preferred due to their ease of retraction and lower draft, which minimize operational interference in harbors. Earlier studies by van der Kolk et al. highlighted the role of bilge keels in roll damping through vortex generation. Bilge keels are advantageous because they are already installed on most vessels for this purpose. Their low height ensures they do not add operational restrictions in ports, making them an effective and unobtrusive option for enhancing stability. In addition to bilge keels, Minai investigated the placement of small, low-aspect-ratio fins, performing systematic tests to evaluate their effectiveness. These fins offer an alternative approach to stability enhancement, particularly in their ability to generate additional side forces at drift angles.

Both bilge keels and low-aspect-ratio fins produce vortices as they generate side forces, which are then convected downstream, influencing the wake flow of the vessel. The effect of drift angles on the wake field has been well-documented in the context of maneuvering operations, providing a foundation for understanding these interactions. The primary objective of this study is to model the influence of bilge keels and low-aspect-ratio fins on the sailing performance of wind-assisted ships. By comparing the results for both types of appendages, this study aims to determine their relative effectiveness. Experimental measurements of forces and maneuvering coefficients will be complemented by flow field analysis in the propeller plane, investigating the impact of flow structures and vortices on the nominal wake. This comprehensive approach will facilitate a thorough evaluation and comparison of the performance of these appendage types.

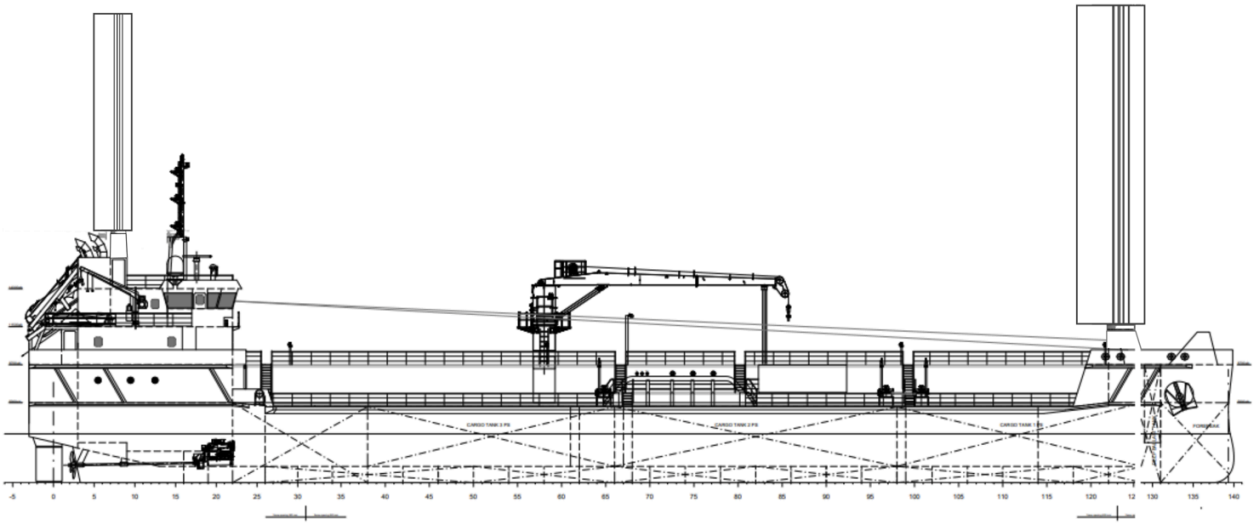


Figure 1 Groot Ship Design Tanker with two Econowind Ventofoils

Main Particulars	
Length over all	90 m
Length between perpendiculars	88.2 m
Beam	18 m
Draft	4 m
Deadweight	3500 t
Main engine power	2x749 kW
VentoFoil (fore)	24x5m
VentoFoil (aft)	16x2.8 m

Table 1 Main particulars for Groot Ship Design Tanker with two Econowind Ventofoils.

A small tanker with wind propulsion systems was developed in collaboration with Groot Ship Design. The vessel has a twin screw arrangement with two rudders, and two medium speed diesel power main engines. The vessel has a particularly large beam and ample transverse stability. Two Econowind Ventofoils are fitted with a large 24x5m device on the forecastle and a 16x2.8m device atop the aft superstructure. This arrangement will enable active control of the aerodynamic center of effort, as described below.

For an experimental assessment of the performance of different types of appendages a hull form with similar characteristics is choses from the Delft Wind-Assist Series which was developed in the recent years by researchers at Delft University of Technology. Representative ship types range from short sea freighters over passenger ferries up to full bodied tankers.

Based on the Ecoliner, designed by Dykstra Naval Architects, the series mostly represents short sea trade vessels and is not valid for Panamax or Cape-sized ships. From this series of 60 hull forms hull number 16 is chosen for the experimental investigation. With its high block coefficient and sharp bilge radius it aids as a geo-sim model with characteristics close to the full-scale model. The appendages to be tested are inspired by former studies from Kolk [] and Minami who independently investigated the potential of bilge keels and fins for wind assisted ships. In the current study a direct comparison of both appendage types is envisaged. The experimentally tested fin and bilge keel configurations are presented in Figure 2

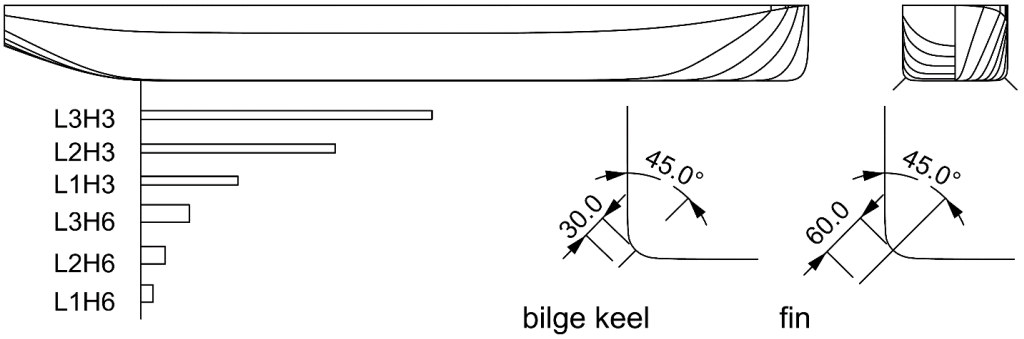


Figure 2: Lines of hull #16 and appendage variations

All appendages positioned as far aft as possible with the aft end located at the aft end of the parallel mid body. Height of bilge keel 30 mm height for fins doubles to 60 mm. No higher appendages tested to limit the influence of operational restrictions.

2. EXPERIMENTAL STUDY

2.1 EXPERIMENTAL SETUP

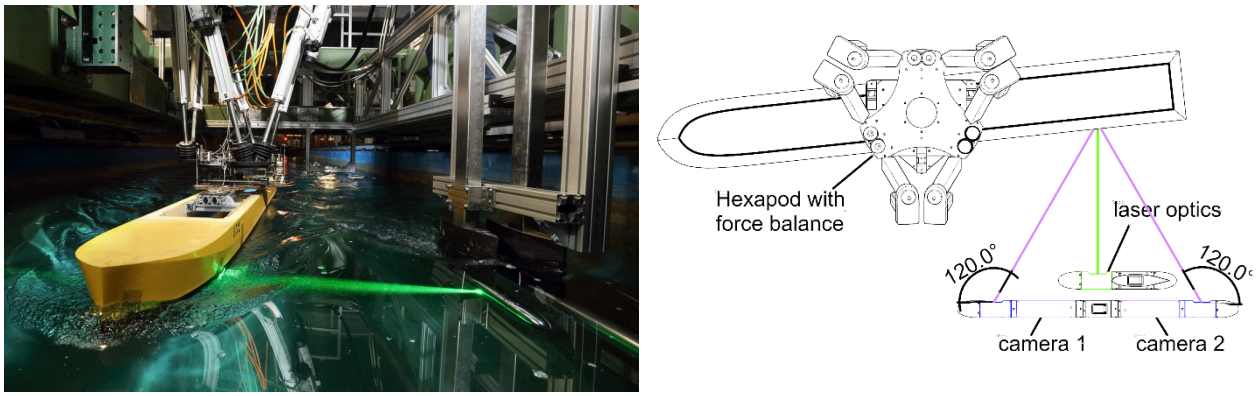


Figure 3: Experimental Setup

The experimental campaign was conducted in the large towing tank at the Ship Hydro-mechanics Laboratory at Delft University of technology. Already used in previous test campaigns by Kolk et al. [1] the model facilitates slits at the bilge in the parallel midship section to fit various types of appendages and to guarantee a quick change of appendages and allow for multiple variations of bilge keel and fin geometries. An overview of the experimental setup is given in Figure 3 (left). For the variation of different leeway angles from 0 to 12 degrees , the model is mounted to a Symmetrie Notus hexapod. Forces and moments are obtained with a 6 component force balance. Although the resistance is expected to be smaller than 10 N, a 50 N transducer is chosen in x-direction to consider possible higher forces in the acceleration and deceleration phase of the carriage. Forces in y-direction and the yaw moment are obtained with two 50 N transducers. As the model is ballasted to half its displacement the vertical force can be measured with 3 transducers of each 200 N. After the assembly of the force

balance a separate calibration is performed for verification of alignment of the single components. To guarantee repeatability of the model alignment, the model is fitted with an alignment frame that enables a quick and precise mounting. The hexapod, force balance and alignment frame are all separately aligned with the towing tank coordinate system using an optical measurement system to guarantee symmetric measurement results at positive and negative leeway angles and reduce the uncertainty due to alignment errors. The total alignment error of the system has been reduced in an iterative procedure to <0.1 degrees.

Flow field measurements are conducted with a stereoscopic underwater particle image velocimetry (PIV) system to measure the velocity field in the propeller plane and determine the influence of drift angles and different types of appendages on the modification of the nominal wake. Flow field measurements conducted in separate runs. While the PIV technique is an optical measurement technique, the model is painted mat black below the waterline to reduce the amount of reflections in the obtained images. The PIV system is mounted to the carriage with a traversing system next to the model and towed together with the model during measurement runs.

The optical measurement setup is described in Figure 3 (right), indicating the position of the cameras and the laser optics used for the illumination of the measurement plane. Particle images are obtained with two LaVision imager MX 4M cameras. Equipped with 28 mm lenses the resulting field of view is approx. 400 x 200 mm with a resolution of 10 px/mm. For the PIV measurements, Polymer particles of 50 µm are distributed in the tank prior to the measurements. For illumination of the measurement plane a double pulse 100 mJ Litron Bernoulli laser with a repetition rate of 50 Hz is used and the laser beam guided through a separate strut underwater, where the light sheet is formed. To capture the complete wake including the windward bilge vortex at higher angles of attack, the flow field is recorded at two transverse positions. At a recording frequency of 50 Hz only few seconds of measurement time are needed to obtain a converged time-averaged velocity field, allowing for the measurement at multiple locations per run. At a carriage speed of 1.09 m/s the time-averaged flow field was obtained at 4 positions per run. A change of measurement location is achieved by traversing the model with the hexapod. Before the measurement at the new location was started it was waited until the flow had been convected by one ship length.

2.2 DATA REDUCTION AND FLOW FIELD PROCESSING

2.2.1 Forces

For the use of the measured data in a performance prediction program, all recorded quantities are non-dimensionalized according to the manoeuvring convention. Measured resistance, side force and Yaw moment are non-dimensionalized using constant hull parameters, such as the ship's length L and draft T. As already described in Kolk et al. [1] the usage of fixed parameters for the hull geometry will introduce small inconsistencies in the calculation of the effective draft, as the change of planform area due to different appendages is not included. Figure 4 shows the obtained dimensionless resistance and side force and their uncertainties for the bare hull and one bilge keel and fin configuration with equal surface area.

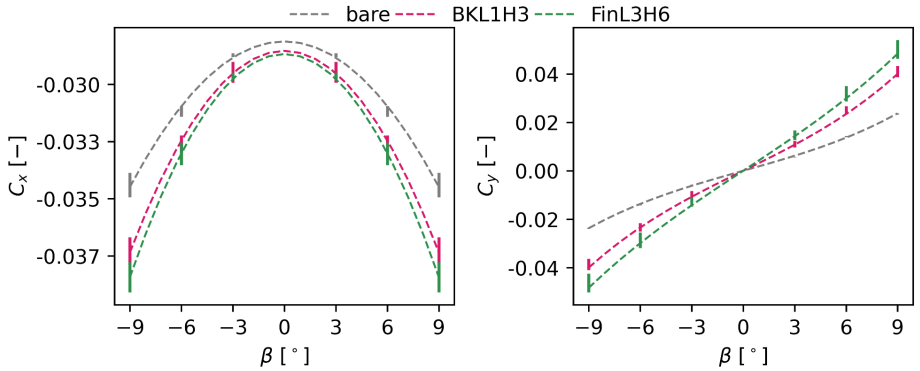


Figure 4: Dimensionless resistance and side force for bare hull and appended cases

While the bare hull case is highly symmetrical, the appended cases show larger differences between positive and negative leeway angles. Although good results are obtained for the bare hull case, this can be attributed to small inaccuracies in the mounting procedure of the appendages or manufacturing uncertainty of the mounting slits. According to the manoeuvring convention, the obtained forces and moments are decomposed using a second-order model for resistance and third-order models for side force and yaw moment.

$$C_X = X_{\beta\beta}\,\beta^2 + C_{XO} \quad \#(4)$$

$$C_Y = Y_\beta \beta + Y_{\beta\beta\beta} \beta^3 \#(5)$$

$$C_N = N_\beta \beta + N_{\beta\beta\beta} \beta^3 \#(6)$$

The dashed line in Figure 4 shows the fitted models for resistance and side force. Course stability and performance of the appendages can be characterized with the determination of the centre of lateral resistance (CLR). The centre of lateral resistance relates the yawing moment to the side force and describes the centre of pressure of the hydrodynamic forces. It is measured from midship position.

To guarantee yaw balance and counteract the destabilizing Munk moment at leeway angles, the CLR needs to be well aligned with the aerodynamic centre of effort to avoid any excessive action from the rudder. In the context of sailing yachts the position of the CLR is a key design constraint and its influence on the vessel performance is extensively discussed in Claughton et al.

2.2.2. Flow field calculation

The stereo camera configuration allows for a determination of the full 3-component velocity vector field in the measurement plane. After the application of a mask for the ship hull, the instantaneous vector field is obtained in multiple correlation iterations with a final correlation window size of 32x32 pixels. With the interrogation windows overlapping by 75 %, the final vector grid has a resolution of 0.8 mm resulting in a total size of the vector grid of 524x312 vectors. Being interested in the time-averaged quantities of the flow field, a robust outlier detection is applied in between passes using a 4-pass regional median filter to reject groups of spurious vectors. The temporal average of all quantities is obtained from 300 successive images. At 1.09 m/s time in between laser pulses dt .. results in a freestream pixel shift of … pixels.

To completely capture the wake field at all leeway angles, the velocity field is obtained at two transverse positions and stitched using Radial basis function (RBF) interpolation in the overlapping region. Figure 5 shows an example of the obtained velocity fields in …

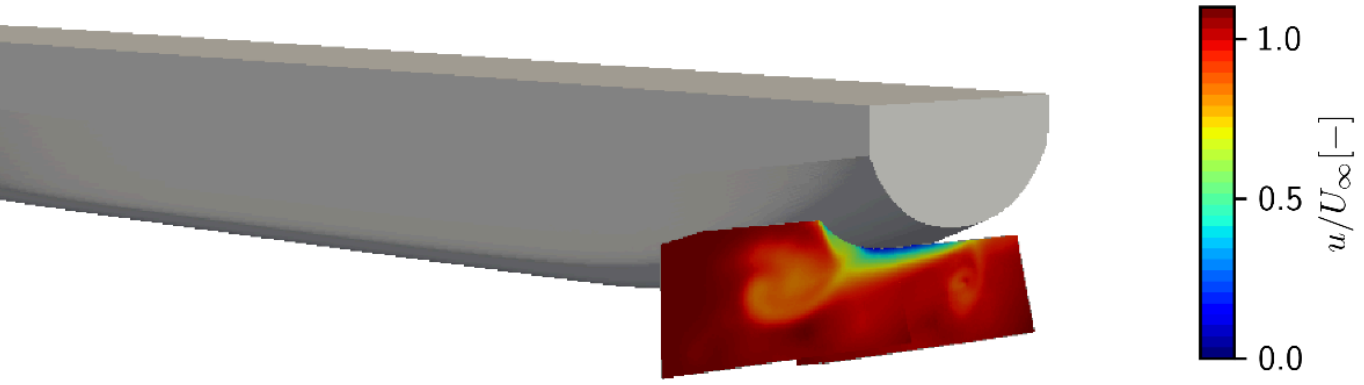


Figure 5: Example of the measured flow field at 9 degrees leeway

To characterize the inflow of the drift angles on the propeller inflow, the nominal wake fraction can be calculated according to

$$w_Ax = 1 - 1/V_s \ [(\int_(d/2)\^(D/2) \int_0\^2\pi V_x\,(r,\theta) r d\theta dr)/(\int_(d/2)\^(D/2) \int_0\^2\pi\, r d\theta dr)] \#(10)$$

which describes the change of the axial velocity in the propeller plane with respect to the ship speed. A reduction of the axial velocity in the propeller plane will result in an increased axial wake fraction. Next to the change of axial velocity in the propeller plane, the average amount of rotation in the propeller plane due to pre-swirl is characterized by the integration of the tangential velocities with respect to the propeller shaft axis.

$$n_(pre - swirl) = [(\int_(d/2)\^(D/2) \int_0\^2\pi\ (- V_t\,(r,\theta))/2\pi r\, r d\theta dr)/(\int_(d/2)\^(D/2) \int_0\^2\pi\, r d\theta dr)] \#(11)$$

3. EXPERIMENTAL RESULTS

3.1 FORCES

Before analysing the effect of the different appendages in an operational scenario, the hydrodynamic performance of single appendages is compared using the experimentally obtained forces. For a better comparison of the forces and moments, the bare hull forces and moments have been subtracted. The influence of the appendages on the change of resistance, side force and moment with changing leeway angle is presented in Figure 6. For both, the bilge keels and the fins, ΔC_X shows a non-linear increase of drag with leeway angle. Due to their large surface area, the bilge keels produce the largest increase of resistance with respect to the bare hull values. However, comparing the shortest bilge keel BKL1H3 and the longest fin FinL3H6 which have the same surface area, the fin has a higher resistance. This can be attributed to the height of the fin extending out of the boundary layer in contrast to the bilge keel which operates in the boundary layer and experiences a lower inflow velocity.

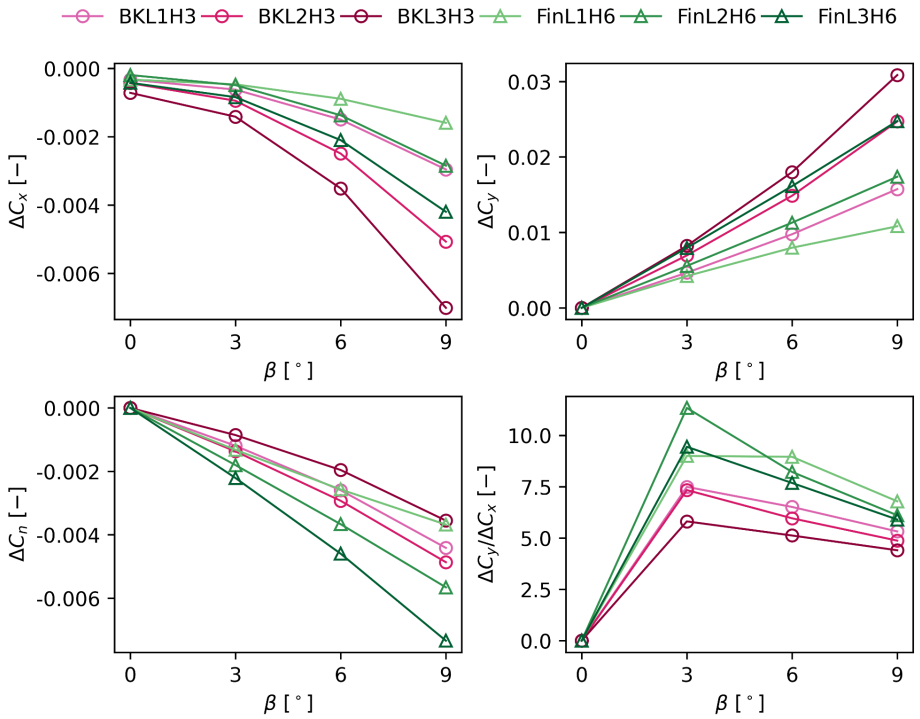


Figure 6: Relative change of resistance, side force, yaw moment and lift over drag ratio for tested appendage configurations

A clear difference between both appendage types can be seen for the side force contribution. While the side force increases non-linear with increasing leeway angle, the fins are characterized by a linear increase of side force with leeway angle. Only the results for the shortest fin deviate from this trend and show a decreasing slope at higher angles of attack. . This might be due to the low Reynolds number of $3.5e\hat{}4$ where early flow separation causes a reduction of lift. Again, the longest bilge keel produces the largest side force. However, comparing again BKL1H3 and FinL3H6 which have the same surface area, the fin creates a significantly larger side force. Due to the non-linear characteristic of the bilge keel with a small slope at small leeway angles, largest differences can be found at small drift angles where the fin produces up to 30% more lift. The large differences can be explained with the different lift generation mechanisms of both systems. While the fin has the characteristics of a typical hydrofoil, the lift generation mechanism of the bile keel is based on flow separation and generation of vortices.

Clear differences between both types of appendages can be also identified for their production of a stabilizing yaw moment. Due to the geometric characteristics of the fins, the centre of effort can be located further aft, resulting in a much higher moment generated by those appendages. For the Bilge keel again a much smaller slope is seen for small angles of attack. Due to the forward shift of the centre of effort the moment increase between BKL1H3 and BKL2H3 is only marginal . Interestingly for the longest bilge keel BKL3H3 even a reduction of the generated yaw moment is obtained. The efficiency of a wing is usually characterized by the ratio of lift and drag. Figure … shows the lift over drag dependency on the leeway angle. With a maximum efficiency around 3 degrees for all appendages, the fin type appendages clearly outperform the bilge keels. Treating FinL1H6 as an outlier due to the low Reynolds number for both appendage types a reduction of efficiency with decreasing aspect ratio can be seen.

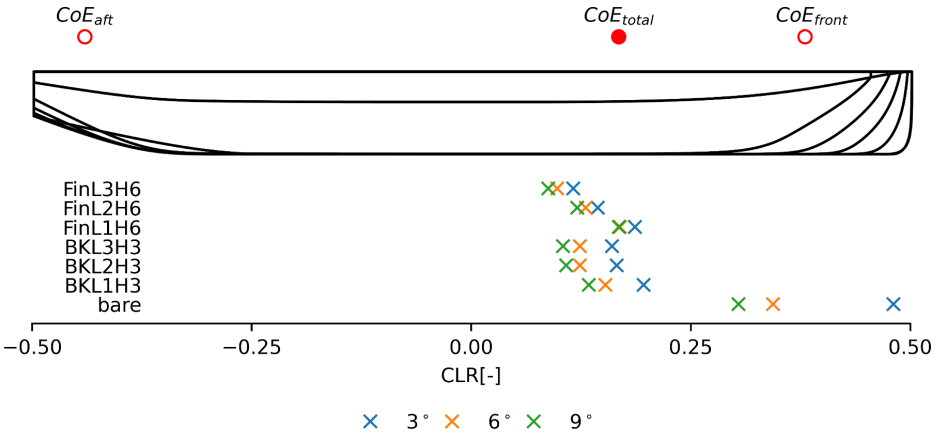


Figure 7: Centre of lateral resistance and longitudinal position of the geometrical centre of effort of the Ventofoils for bare hull and appended cases.

As already mentioned in Section 2.2.1, the centre of lateral resistance needs to be located at the longitudinal position of the aerodynamic centre of effort for the ship to sail at a straight course. Figure 7 shows the calculated CLR for the bare hull and all tested appendages. With the bare hull CLR located close to the bow, all appendage types succeed in moving the CLR towards the back. However, the bilge keels show a much larger variation of CLR position over varying angles of attack. While for the fins, the CLR can be efficiently moved backwards with increasing surface area, the CLR position for increasing bilge keel length does not significantly improve with increasing bilge keel length.

3.2 FLOW FIELD MEASUREMENTS AND WAKE FRACTION CALCULATION

Flow field measurements in the propeller plane are conducted for three selected test cases, bare hull, the shortest bilge keel variant BKL1H3 and the longest fin FinL3H6 with equal surface area. The leeway angle was varied between 0 and 9 degrees. As described in Section 2.1 the flow is measured at two transverse positions and the flow field is stitched together to capture the wake in the virtual propeller planes and the side vortex which develops with increasing leeway angles on the windward side of the hull. Figure 8 shows an overview of the measured flow field for all tested cases and conditions. The circles indicate the position of the virtual propeller location for evaluation of the wake fraction and pre-swirl calculation. For a later analysis of the axial wake fraction and pre-swirl the measured velocities are translated to the ship coordinate system. While the contours represent the axial velocities, the quiver plot shows the in-plane velocity components.

For the bare hull the formation of the forward side vortex with increasing leeway angle on the windward side is clearly visible. The shadowing effect of the hull leads to a decrease of axial velocity in the propeller plane on the windward side. At 9 degrees, when the side vortex has moved further away from the hull, the axial velocity is again increasing in the propeller plane. Having a simplified aft ship geometry without skeg, this velocity increase is believed not to occur on a more realistic aft ship geometry. For the leeward propeller, the shadowing effect of the hull will get smaller with increasing leeway resulting in a less disturbed inflow into the propeller plane.

Comparing the flow field to the appended cases, for both types of appendages an interaction of the appendage wake with the side vortex can be noticed. However, the flow in the windward propeller plane is not affected by the tested appendage configurations. Looking at the wake fraction in Figure 9, it follows the same trend as obtained for the bare hull case. At higher leeway angles the formation of a vortex from both types of appendages can be noticed on the leeward side. Especially at the 6 and 9 degrees cases a modification of leeward propeller inflow can be noticed due to the appendage wake resulting in an increase of wake fraction for these angles compared to the bare hull case. Due to the smaller height of the bilge keel, the vortex for this appendage is located closer to the hull compared to the vortex formed at the tip of the fin with the vortex axis almost at the centre of the propeller plane. Due to the scaled velocity vectors, the vortices can be clearly identified in the measured flow field. Looking at the calculated pre-swirl in the propeller planes in Figure 10, their contribution to generating additional pre-swirl can be neglected. In general, due to the simplified aft ship geometry no significant pre-swirl is generated for all tested cases. As the calculated pre-swirl is an integral parameter, the local effect of the vortices on the propeller performance is not captured and needs further investigation.

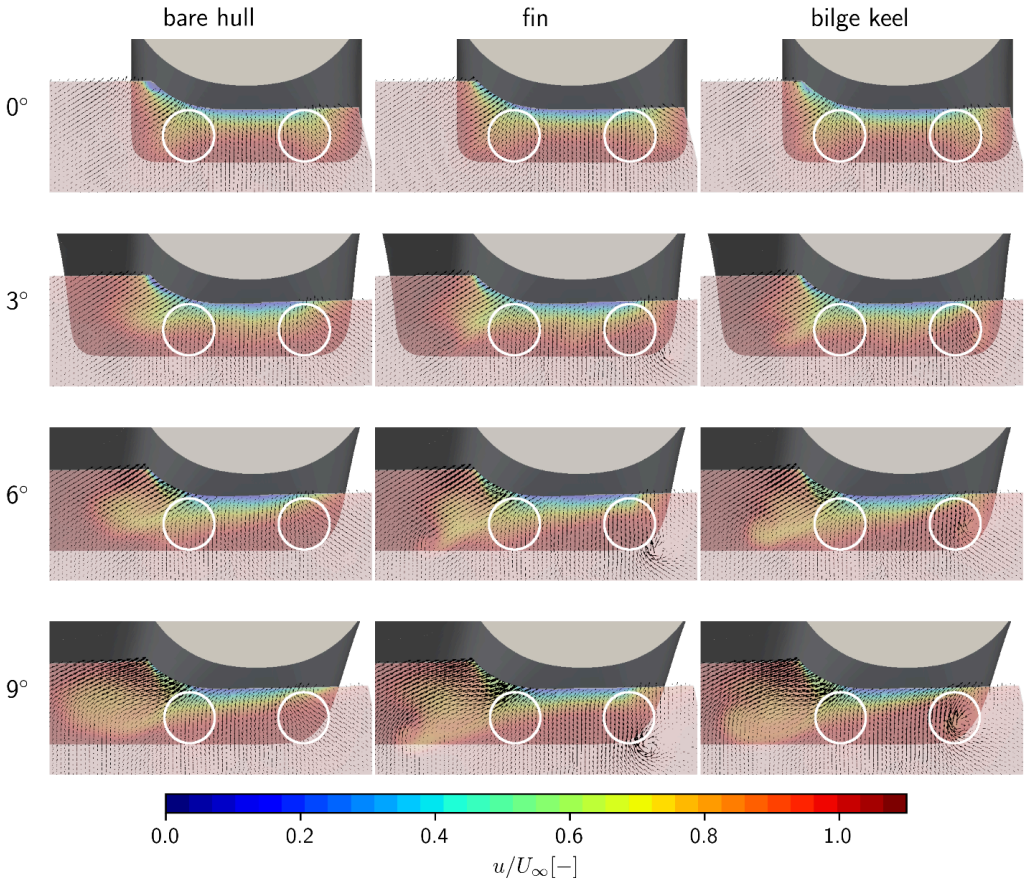


Figure 8: Obtained velocity fields in the wake and propeller planes (white circles) for bare hull and cases with appendages L3H6 and L1H3

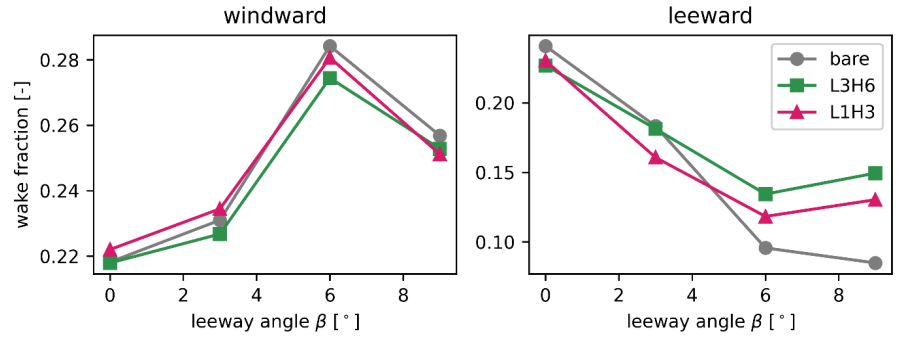


Figure 9: Wake fraction dependency on leeway angle

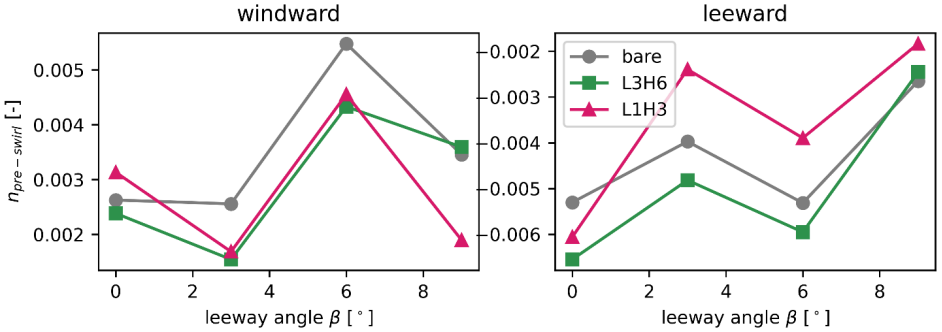


Figure 10: Pre-swirl dependency on leeway angle

4. OPERATIONAL EFFICIENCY

4.1 ALBATROS DIGITAL SHIP MODEL

The Albatros Digital Ship Model is a state-of-the-art simulation tool that provides an assessment of the impact of the appendage geometries on the performance of the wind assisted ship. The model integrates a powerful methodology that combines Reynolds-averaged Navier-Stokes (RANS) computational fluid dynamics (CFD) with advanced machine learning algorithms, described in detail in Mason et al 2023 and van der Kolk et al 2020. The model is deployed on a modern web-based infrastructure, featuring a cloud-native modelling engine that includes rapidly scalable computing resources. This architecture allows for efficient processing of large datasets and complex simulations, ensuring that users can quickly obtain accurate results. The model's flexibility extends to its integration with client data and services, offering bespoke preconditioners and plug-ins that can be customized to meet specific needs.

4.1.1 INTEGRATION WITH EXPERIMENTAL DATA

A key feature of the Albatros Digital Ship Model is integration of empirical data from towing tank experiments or monitoring data sources. The manoeuvring coefficients and wake fraction outlined in Section 3 are that are incorporated to assess the effects of different appendage geometries on ship performance. A new implementation of a wake fraction response surface for port-side and starboard-side propellers has been developed. The axial wake fraction effects induced by appendages like bilge keels and low-aspect-ratio fins are brought to full scale using ITTC formulae and represented in the hull efficiency using multi-variate mappings derived from the experimental data.

4.2 ASSESSMENT OF APPENDAGE OMETRIES

The impact of appendage geometries is assessed with two principal quantities: the aerodynamic centre of effort (COE) and P_WPS which is non-dimensionalized using True Wind Speed, described below.

4.2.1 AERODYNAMIC CENTER OF EFFORT (COE)

The COE is defined as the longitudinal position of the aerodynamic thrust vector, which provides the aerodynamic control needed to balance the helm of the vessel. Any difference between the COE, the hull's center of lateral resistance (CLR), and the windage of hull and superstructure must be compensated by the rudder. This compensation is a limiting constraint, as excessive rudder use can reduce efficiency and increase fuel consumption. To facilitate comparison, the COE value is normalized by the length between perpendiculars (Lpp), aligning it with the CLR definition.

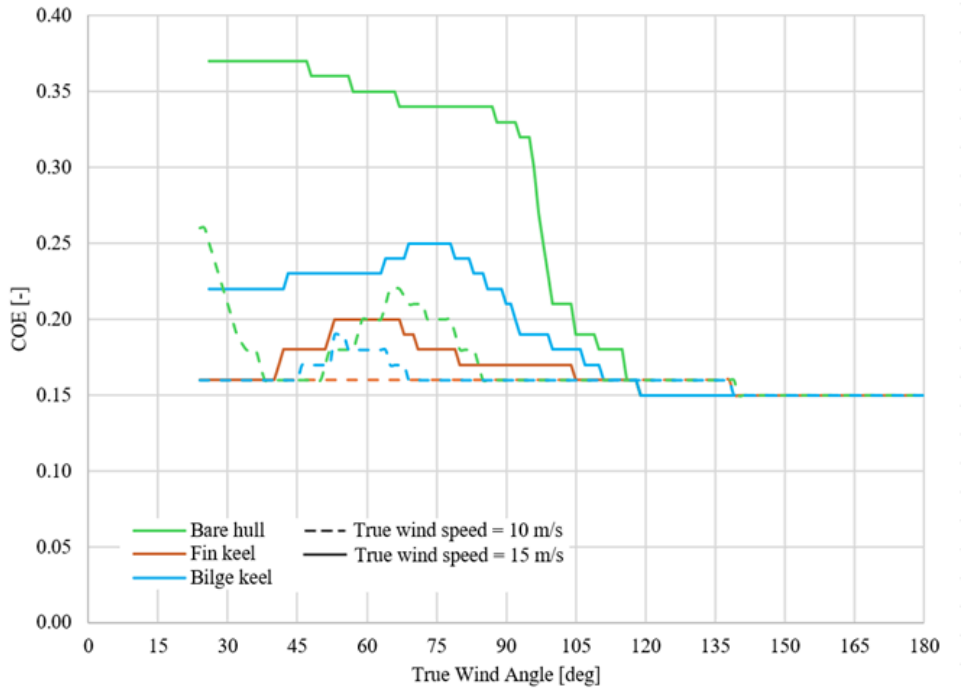


Figure 11Aerodynamic COE for Bare hull, Fin keel, and Bilge keel configurations showing response at True Wind Speed=10 m/s (dashed line) and 15 m/s (solid line).

Simulation results for the aerodynamic centre of effort are presented in Figure 11 showing performance of the three configuration tested at 10 m/s (dashed line) and 15 m/s (solid line). We see that both the bilge keel and fin keel show an improved performance compared with the bare hull, where one can observe that the fin keel arrangement does not depower the aft sail at wind speed = 10 m/s. On the other extreme, at true wind speed = 15 m/s, upwind vessel sailing balance requires complete de-powering of the aft sail on the bare hull case (the normalize position of the forward sail is 0.38). Introduction of bilge and fin keels has improved the upwind sailing performance especially at high wind speeds. The geometric centroid of the WPS installation is at 0.17 with respect to LPP/2 (normalized ordinate).

4.2.2 WPS Power P_WPS

The quantity P_WPS, which is the main-engine-equivalent propulsive power as defined by EEDI with added resistance term associated with the sailing condition, is furthermore non-dimensionalised using the available wind power. This facilitates comparative analysis across different wind speeds, WPS installations, and ship sizes.

This quantity is calculated as follows:

P_WPS: Represents the effective propulsive power from the wind-assisted system, calculated using the EEDI formula including ΔR_WPS which is the extra resistance introduced due to steady drift, heel, rudder angles, and the added appendages at zero degrees (if applicable). The interaction between the appendage wake and the hull efficiency is incorporated in this quantity as well.using an average of the port-side and starboard side value.

$$P_WPS = V_s/eta_D(F_{WPS} - \Delta R_{WPS}) - P_{WPS,in}/eta_{Gen}$$

The simulations are conducted for a ship speed equal to 11 knots, or 5.66 m/s. A non-dimensionalization is adopted using the vessel LOA and WPS span as reference area. Other definitions for reference area may be considered.

$$P_WPS \; *= P_WPS \; / \; (1/2 \; \rho_air \; (LOA{\cdot}Span)TWS\text{^}3)$$

Hens this ratio quantifies the proportion of wind-over-deck that is converted into useful main-engine-equivalent propulsive power and can therefore be understood as an overall efficiency metric for the WPS installation.

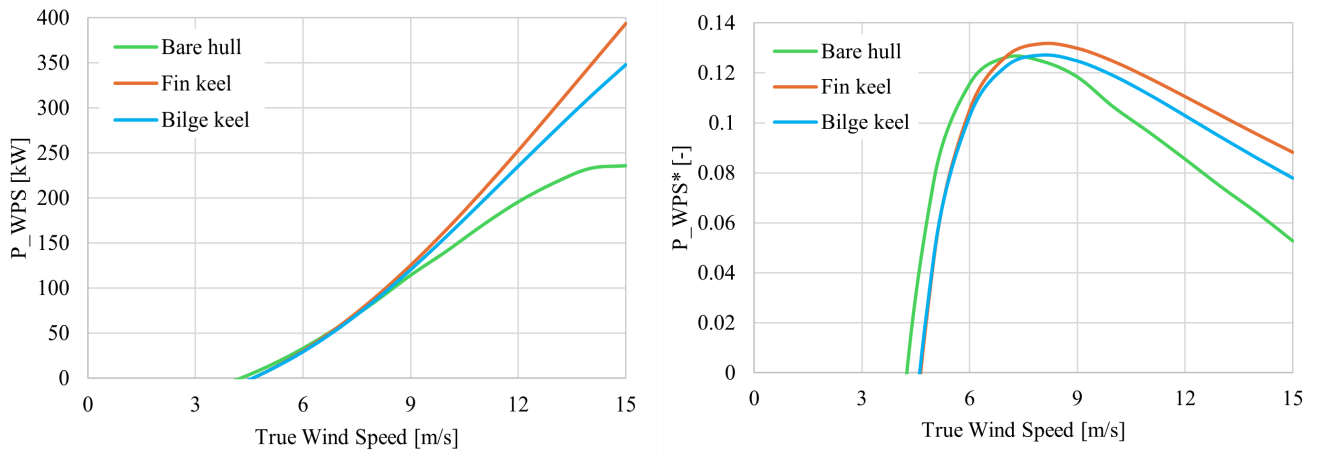


Figure 12: Wind-assist power expressed as main-engine-equivalent propulsive power (left) and as non-dimensional value (right).

The performance of the two appendage types are first considered on a circular-random basis, which is an averaged performance over an equal distribution of wind angles. The results show in Figure 12 (left) illustrate the limiting influence of course stability of the Bare hull case, where P_WPS reaches a maximum contribution of approximately 235 kW. Both Fin keel and Bilge keel appendage arrangements show clear improvements here, with the Fin keel case reaching 390 kW for 66% increase compared with Bare hull. The Bilge keel reaches a maximum of 350 kW or and increase of 49%. Performance gains are maintained at lower true wind speeds to about 7 m/s for the Fin keel and about 7.5 m/s for the Bilge keel (Figure 12 right), where improvements of the hydrodynamic induced drag are responsible rather than improved course keeping. Finally, at wind speeds below 7 m/s the added appendage resistance for both keel geometries outweighs any benefit to the

sailing performance. The Fin keel provides additional 8% performance on aggregate compared with 4% for the Bilge keel over the wind speed range 7-10 m/s.

ΔP_{WPS} [kW]
(Fin keel - Bare hull)

Wind angle [deg] \ Wind speed [m/s]	1	3	5	7	9	11	13	15
0	-9.8	-9.8	-9.8	-9.8	-9.8	-9.8	-9.8	-9.8
15	-9.9	-9.8	-8.9	-7.1	-5.1	-3.3	-1.8	-0.8
30	-9.7	-6.4	-1.4	6.6	22.5	48.6	79.4	114.1
45	-8.8	-6.1	0.6	13.3	40.0	96.7	165.1	241.3
60	-8.9	-5.1	3.9	22.3	69.7	153.1	263.7	442.3
75	-9.0	-4.9	3.0	18.8	67.3	158.4	322.1	575.6
90	-9.2	-5.7	-0.6	8.9	33.3	98.2	255.0	515.5
105	-9.3	-7.2	-3.7	1.1	9.7	33.1	93.0	276.1
120	-9.5	-8.5	-6.9	-4.7	-1.6	2.3	13.1	36.9
135	-9.7	-9.3	-9.0	-8.7	-8.2	-7.5	-6.4	-5.3
150	-9.8	-9.7	-9.8	-9.9	-9.9	-9.9	-9.7	-8.5
165	-9.9	-9.9	-9.9	-9.9	-9.7	-8.6	-5.4	2.4
180	-10.0	-10.0	-10.0	-9.9	-9.3	-6.8	-0.6	10.0

ΔP_{WPS} [kW]
(Bilge keel - Bare hull)

Wind angle [deg] \ Wind speed [m/s]	1	3	5	7	9	11	13	15
0	-7.8	-7.8	-7.8	-7.8	-7.8	-7.8	-7.8	-7.8
15	-7.7	-7.6	-7.2	-6.4	-5.5	-4.7	-4.1	-3.6
30	-7.6	-5.6	-2.8	2.0	13.2	31.9	48.3	65.4
45	-7.1	-5.5	-1.6	5.9	25.1	68.2	109.7	146.1
60	-7.2	-4.9	0.5	13.5	49.9	107.1	178.3	314.5
75	-7.2	-4.8	0.0	10.5	51.2	113.8	229.4	413.0
90	-7.3	-5.3	-2.2	3.8	22.5	74.4	195.1	379.3
105	-7.4	-6.2	-4.1	-1.1	5.1	24.5	71.7	218.9
120	-7.5	-7.0	-6.1	-4.7	-2.7	0.0	8.7	27.2
135	-7.6	-7.4	-7.3	-7.3	-7.2	-6.9	-6.4	-5.8
150	-7.7	-7.7	-7.8	-8.0	-8.2	-8.6	-8.9	-8.7
165	-7.7	-7.8	-7.8	-7.9	-7.9	-7.4	-5.7	-1.0
180	-7.8	-7.8	-7.8	-7.8	-7.5	-6.0	-2.3	4.2

Table 2Improvements in WPS power for Fin (left) and Bilge (right) keel configurations.

Finally, wind-assist power is presented for specific wind angles and directions relative to the Bare hull values in Table 2 above. A gradient color key is applied with 2-20 kW: light green, 20-200kW: green, and >200kW dark green, showing that the global response is broadly similar with the Fin keel reaching between 40% higher performance in light conditions to 25% in heavy conditions. The Fin keel arrangement is significantly better performing at small angles as can be expected, superior to the Bilge keel by between 30%-40% for wind speeds above 7 m/s.

5. CONCLUSIONS

- Both the Fin keel and Bilge keel bring substantial improvements to the sail-carrying qualities of the vessel in heavy air.
- Cross-over wind speed for Fin keel was 7 m/s compared with approximately 7.5 m/s for the Bilge keel.
- Performance improvements observed in two mechanisms: improved course keeping for heavy conditions at wind angles between 60-110 degrees and smaller hydrodynamic induced resistance for light conditions where wind speeds greater than cross-over wind speed.
- Variations of maximum 7% seen for delivered power efficiency between windward and leeward propeller, occurring for heavy conditions only.

6. ACKNOWLEDGEMENTS

The Authors would like to thank Bart Groot and Groot Ship Design for their help developing the concept WPS vessel.

7. REFERENCES

1. van der Kolk NJ, Akkerman I, Keuning JA, Huijsmans RHM (2021) Low-aspect ratio appendages for wind-assisted ships. Journal of Marine Science and Technology (Japan) 26:1126–1143 Doi.org/10.1007/s00773-020-00777-8
2. Minami Y, Nimura T, Fujiwara T, Ueno M (2003) Investigation into Underwater Fin Arrangement Effect on Steady Sailing Characteristics of a Sail Assisted Ship.
3. Schot JJA, Eggers R (2019) Wind Propulsion, 15 th-16 th.
4. Mason J, Larkin A, Bullock S, van der Kolk NJ, Broderick JF (2023) Quantifying voyage optimisation with wind propulsion for short-term CO2 mitigation in shipping. Ocean Engineering, Volume 289, Part 1, https://doi.org/10.1016/j.oceaneng.2023.116065.
5. Claughton, A. & Pemberton, R., "Hull–Sailplan Balance, "Lead" for the 21st Century," 22nd International HISWA Symposium on Yacht Design & Yacht Construction, Amsterdam 2012.

6. van der Kolk NJ. Sailing efficiency and course keeping ability of wind-assisted ships. PhD thesis, Delft University of Technology. 2020

8. AUTHORS BIOGRAPHY

Gunnar Jacobi holds the current position of a research associate at Delft University of Technology. The Author is responsible for [brief job description]. The Author's previous experience includes [previous experience relevant to the paper], etc. The authors' names should be in bold.

Nico van der Kolk holds the current position of Naval Architect at AlbatrosDigital. The Author is responsible for [brief job description]. The Author's previous experience includes [previous experience relevant to the paper], etc. The authors' names should be in bold.